Supporting Information

A seal glass should sinter well in order to avoid the formation of voids and reduce the amount and size of strength flaw populations that limit the mechanical strength and the reliability of the resultant GC. Gehlenite and akermanite belong to melilite group of silicates and form continuous solid solutions. Due to the high content and the mobility of alkaline–earth ions in these glasses, intermediate crystalline phases form upon sintering, thus hindering the complete densification in the resultant GCs. In our previous study we attempt control the mobility of CaO and avoid the formation of meta–stable crystalline phases by adding to the glass composition different amounts of the low melting Bi_2O_3. Enhanced sintering was only observed in the presence of small amount of Bi_2O_3. In the present work, substitution of Sr for Ca and B for Al in melilite composition (MB–1)[1] was attempted and the effect of adding different amounts of ZrO_2 on glass properties such as structural, thermal and mechanical were investigated. To avoid impair of technological properties of parent glass a large amount of ZrO_2 (> 5 mol. %) was not used in the present investigation.

S1: Experimental

High purity powders of SiO_2 (>99.5%), $CaCO_3$ (>99.5%), $MgCO_3$ (BDH chemicals, UK, >99%), $BaCO_3$ (Sigma Aldrich, 99.9%), Al_2O_3 (Sigma Aldrich, >98%), La_2O_3, $SrCO_3$ (Sigma Aldrich, 99.9%), H_3BO_3 (>99.5%), Bi_2O_3 (Sigma Aldrich, 99.9%), and ZrO_2 (Sigma Aldrich, 99%) were used. Homogeneous batch mixtures of 100 g (Table 1), obtained by ball milling were preheated at 1100 ºC for 5 h for decarbonisation and then melted in Pt crucibles at 1585 ºC for 2 h, in air. More experimental details were described elsewhere.[1-3] The amorphous nature of glasses was confirmed by X–ray diffraction (XRD) analysis (Rigaku Geigerflex D/Max, Tokyo, Japan; C Series; Cu K_α radiation; 2θ range 10º–80º; step 0.02 $^o s^{-1}$).

The sintering behavior of the glass powders was investigated using a side–view hot stage microscope (HSM) EM 201 equipped with image analysis system and 1750/15 Leica electrical furnace. The values of the crystallization onset temperature (T_c) and peak temperature of crystallization (T_p) were obtained from the DTA thermographs using differential thermal analysis (DTA–TG, Setaram Labsys, Setaram Instrumentation, Caluire, France) at a heating rate of 5 K min^{-1}. The detailed experimental procedures were previous described.[1-3] The mechanical properties were evaluated by measuring the three–point bending strength of rectified parallelepiped bars of sintered GCs (Shimadzu Autograph AG 25 TA, Columbia, MD; 0.5 mm min^{-1} displacement). The values of CTE for GCs were obtained from dilatometry measurements carried out on prismatic samples with a cross section of 4 mm × 5 mm (Bahr Thermo Analyze DIL801 L, Hullhorst, Germany; heating rate 5 K min^{-1}).

Rectangular bars with dimensions of 4 mm × 5 mm × 50 mm were prepared by uniaxial pressing (80 MPa). In order to study the shrinkage behavior and density of resultant GC sealants, glass powder rectangular bars were sintered at 850 ºC for 1 h. To study the stability of the above mentioned properties, the GCs sintered at 850 ºC for 1 h were further heat treated at 800 ºC for 500 h at 5 K min^{-1}. The linear shrinkage during sintering was calculated from the difference in the dimensions between the green and the sintered bars. Archimedes' method (i.e., immersion in diethyl phthalate) was employed to measure the apparent density of the sintered GCs. The bending strength of the GCs sintered at 850 ºC for 1 h was measured (Shimadzu Autograph AG 25 TA, Columbia, MD; 0.5 mm min^{-1} displacement) and the mechanical reliability was tested by applying the well–known Weibull statistics to the experimental data.[4]

Infrared spectrum of glass was obtained using an Infrared Fourier spectrometer (FT–IR, model Mattson Galaxy S7000, USA). For this purpose, the glass powder was mixed with KBr in

the proportion of 1/150 (by weight) and pressed into a pellet using a hand press. 64 scans for background and 64 scans per sample were made with signal gain 1. The resolution was 4 cm^{-1}.

S2: Physical and thermal properties of glasses

Table S1: Density (g cm^{-3}), molar volume (MV) (cm^3 mol^{-1}), Excess molar volume (EMV) (cm^3 mol^{-1}), and CTE ($\times 10^{-6}$ K^{-1}) (200–700 ºC) of glasses

	Density	MV	EMV	CTE	T_{ds}
Zr–0	3.240±0.004	20.88±0.03	0.81±0.02	11.0	752
Zr–1	3.265±0.002	20.68±0.01	0.63±0.01	10.7	755
Zr–2	3.284±0.003	20.51±0.02	0.49±0.02	10.7	763
Zr–3	3.320±0.001	20.25±0.01	0.25±0.01	10.5	773
Zr–4	3.342±0.003	20.07±0.02	0.11±0.02	10.6	781

All the five glass compositions were prone for easy casting after 2 h of melting at 1585 ºC, resulting in homogeneous and transparent glasses. Among the various physical properties of the glass, density is the most important and sensible to the glass composition. The variation of the density and molar volume by the ZrO_2 addition, reported in Table S1, shows a clear increase in the experimental density as a function of the ZrO_2 concentration in the glass matrix. The increasing density values of the glass matrix induced by the incremental amounts of added zirconia reflect the trend expected from the incorporation of a denser oxide. In general, the addition of extra ions in the glass structure results in the modification of the density of the final material. In particular, this effect is strongly related to the mass of the added ions as a function of their content in the base glass. The enhancement in glass density with added amount of ZrO_2 correlates well with the observed decreasing trend for the molar volume (Table S1). The closer packing of the glass structure explains the network forming role of ZrO_2 in the present glass matrix.

The values of softening point temperature (T_s) increased monotonically from 752 to 781 ºC while CTE of the glasses non-significantly decreased with increasing ZrO_2. Thus, the maximum value was revealed for Zr–0 glass (11×10^{-6} K^{-1}) and the minimum for Zr–4 (10.6×10^{-6} K^{-1}). Further, the increasing T_s and the decreasing CTE values also support the network former role played by the Zr atoms in the glass materials, in good agreement with the local structure information gathered from NMR measurements.[5] However, as explained by Lancellotti et al.,[6] the added ZrO_2 does not considerably affect the glass structure, since the addition of species that fill the interstices of the vitreous network will generally increase the density and the corresponding properties of the material.

S3: XRD-Rietvield RIR

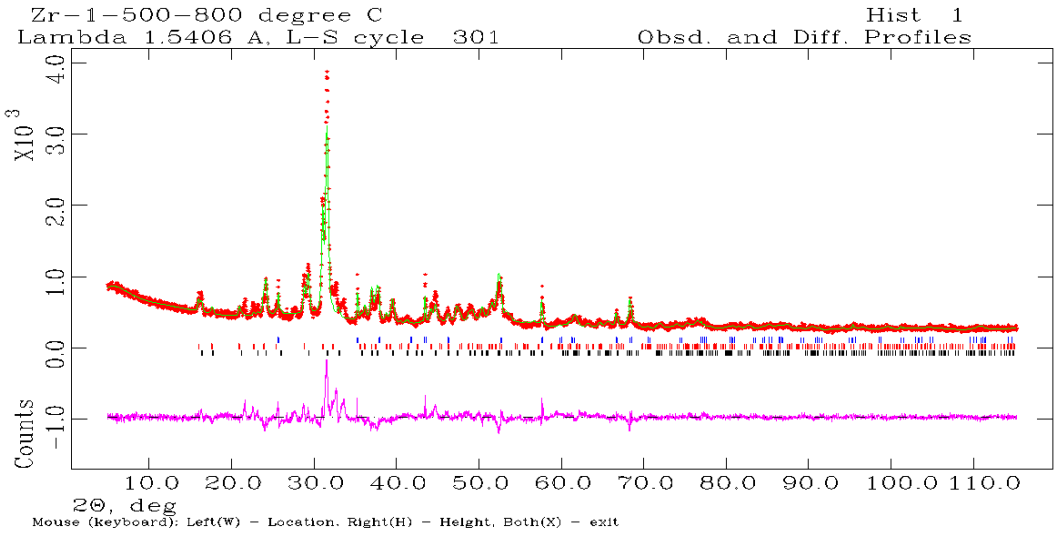

Figure S1: Observed, calculated, and difference curve from the Rietveld refinement of the Zr–1 GC heat treated at 800 ºC for 500 h in air atmosphere.

Fig. S1 shows the fit of a measured XRD pattern of a sintered GC by using the GSAS-EXPGUI software. The difference plot does not show any significant misfits. The differences under the main peaks of akermanite and gehlenite are caused by adjustment difficulties based on crystallinity of phases.

S4: Structural information: Solid state NMR and FTIR

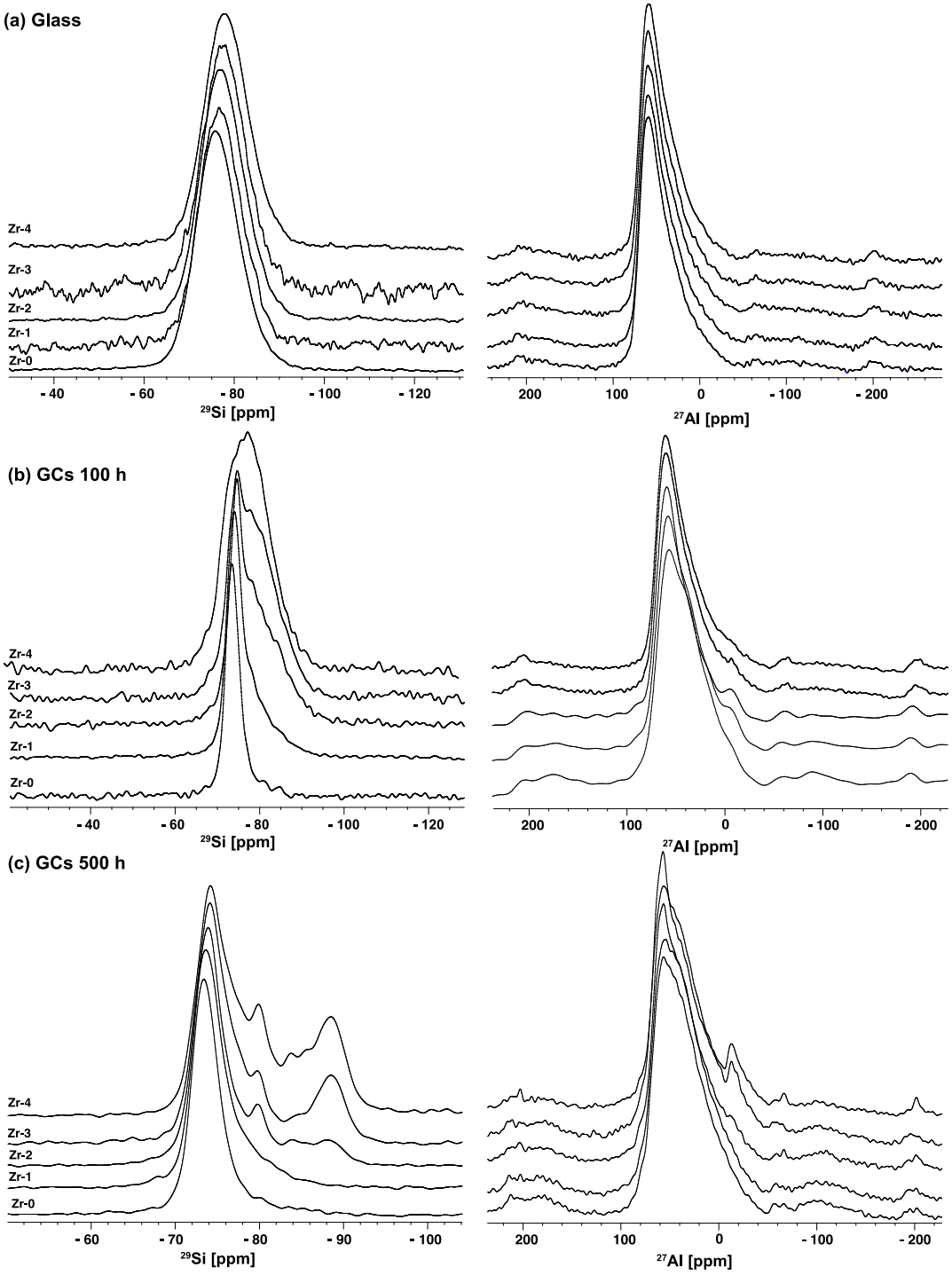

Figure S2. (left) ^{29}Si MAS and (right) ^{27}Al MAS NMR spectra of the Zr-0 to Zr-4 glasses and Zr-0 to Zr-4 GCs sintered at 850 ºC for 100 and 500 h.

Table S2: Quantification of the deconvoluted silicon components from Figure **3**.

Resonance (ppm)	Peak	Area /a.u.	Percentage Area (%)	FWHM (a.u.)
		Zr0		
-73.5	a	n/a	100	4.52
		Zr-2		
-73.8	a	5.00 ± 0.004	74.2	4.65
-77.0	b	0.28 ± 0.013	4.2	2.73
-79.8	c	0.69 ± 0.010	10.2	3.64
-83.8	d	0.26 ± 0.011	3.9	2.35
-85.5	e	0.05 ± 0.007	0.7	2.63
-88.2	f	0.46 ± 0.004	6.8	5.09
		Zr-4		
-74.0	a	4.88 ± 0.002	49.8	4.67
-77.0	b	0.84 ± 0.003	8.6	3.45
-79.9	c	1.37 ± 0.004	14.0	3.89
-83.8	d	0.64 ± 0.004	6.5	3.41
-85.5	e	0.06 ± 0.003	0.6	1.31
-88.2	f	2.00 ± 0.004	20.4	5.40

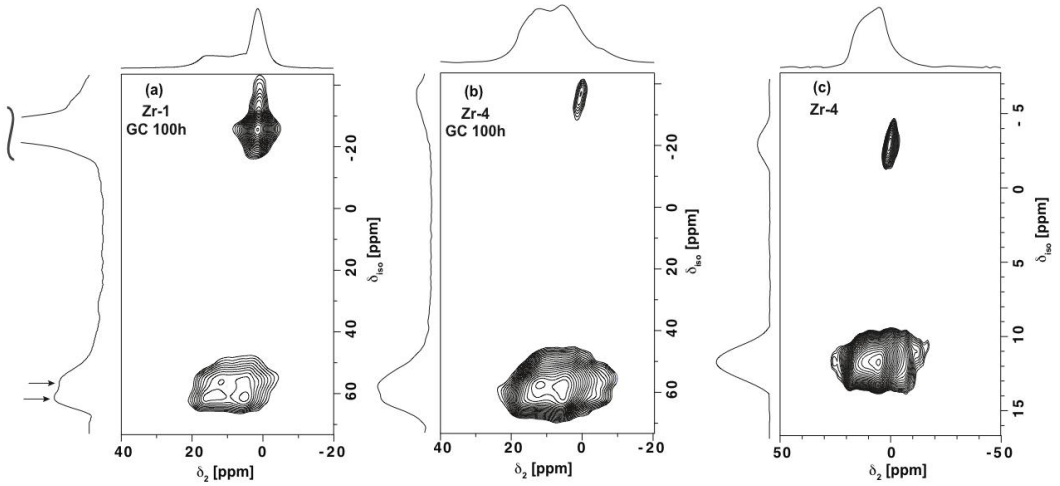

Figure S3. 2D ^{11}B 3QMAS spectra of (a) Zr-1 and (b) Zr-4 GCs samples sintered for 100 h and (c) 2D ^{11}B STMAS spectrum of the Zr-4 glass sample.

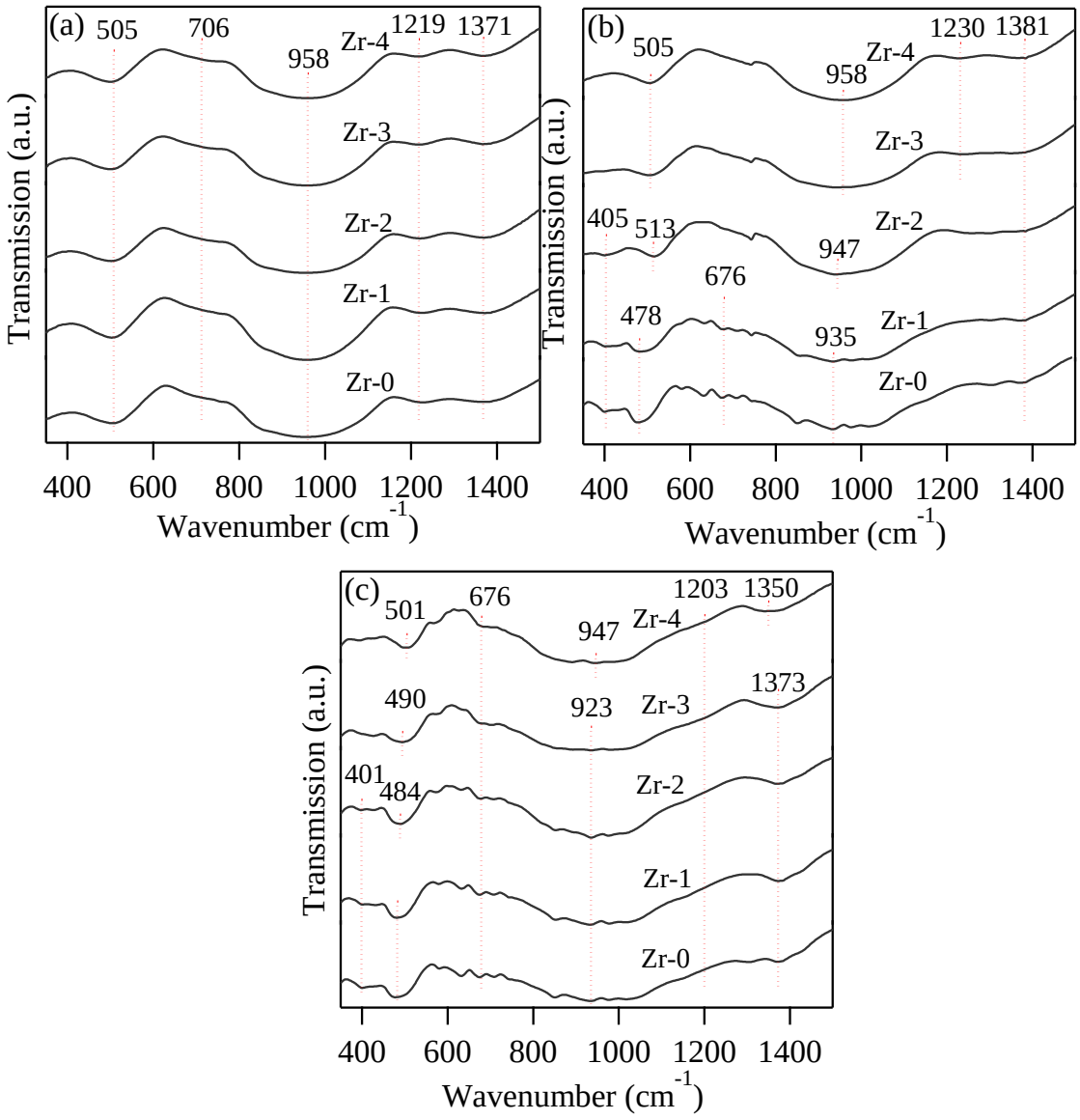

Figure S4: FTIR spectra of (a) investigated glasses and glass–ceramics annealed at 800 °C for (b) 100 h and (c) 500 h

The room temperature FTIR transmittance spectra of the investigated glass is shown in Fig. 1. The glass exhibits four broad transmittance bands in the region of 300 to 1500 cm^{-1}. This lack of sharp feature is an indicative of general disorder in the silicate network mainly due to the wide distribution of Q^n units (polymerization in the glass structure, where n denotes the number

of bridging oxygens) occurring in the glasses. The most intense broad band in the 800–1200 cm^{-1} region indicates the stretching vibrations of Si–O–Si linkages in the SiO_4 tetrahedron unit. The appearance of high intensity broad band at 958 cm^{-1} due to the nonbridging Si–O terminal stretching vibrations, suggest that Q^2 units are highly localised. The band in the 300–600 cm^{-1} region corresponds to bending vibrations of Si–O–Si and Si–O–Al linkages. With respect to the aluminum coordination in glass structure, the presence of transmittance band from medium to strong intensity in the 600–750 cm^{-1} region with the centre of gravity at ~694 cm^{-1} is a typical feature of stretching vibration of the Al–O bond with aluminum ions in Al four coordination. The absorption band in the 1350–1550 cm^{-1} region of the spectrum indicates the existence of three-coordinated boron atoms (BO_3) where as the absorption band in the region 1200 to 1300 cm^{-1} indicates the existence of isolated $(BO_3)^{3-}$ ions. However, as confirmed from ^{11}B NMR studies the existence of BO_4 units, having the characteristic frequency range of 1100-1200 cm^{-1} is difficult from the FTIR spectra because SiO_4 groups have similar vibrational frequency and react with them. The FTIR spectra presented in Fig. S4 of all glass powder compacts sintered at 850 ºC for 1h and at 800 ºC for 100 h, 500 h show the splitting of broad bands into a number of intense and sharp bands. This indicating the crystalline nature of the samples. Further, these results are in accordance with the XRD and NMR studies. With the prolonged heat treatment the appearence of absorption band in the region of 1200 cm^{-1} confirming the existence and the reaction of BO_4 units with the SiO_4 groups in the present glasses.[7]

S5: Glass-ceramic properties: Density, Shrinkage and Weibull statistics

Table S2 presents linear shrinkage, density and Weibull statics results of GCs after sintering at 850 ºC for 1 h and 500 h. Usually, glassy powders in which sintering precedes crystallization result in high shrinkage, dense and mechanically strong GCs.

Table S2: Shrinkage (%), density (g cm^{-3}) and Weibull distrubutions (m and σ_0) measured for the glass–powder compacts after sintering at 850 ºC for 1 h fallowed by at 800 ºC for 500 h.

Composition	Zr–0	Zr–1	Zr–2	Zr–3	Zr–4
Shrinkage (%)					
1 h	13.7±0.5	13.3±0.6	13.3±0.4	13.1±0.5	12.7±0.5
500 h	14.3±0.3	13.8±0.5	14.8±0.4	14.3±0.3	13.0±0.5
Density (gcm^{-3})					
1 h	3.22±0.01	3.25±0.01	3.30±0.01	3.31±0.01	3.34±0.01
500 h	3.22±0.01	3.34±0.01	3.31±0.01	3.35±0.01	3.35±0.01
Weibull modulus					
1 h	6.5	7.2	10.75	7.4	10
500 h	6.7	10.6	7.57	9.7	7.3
Weibull strength (MPa)					
1 h	118	113	108	111	102
500 h	124	120	106	112	102

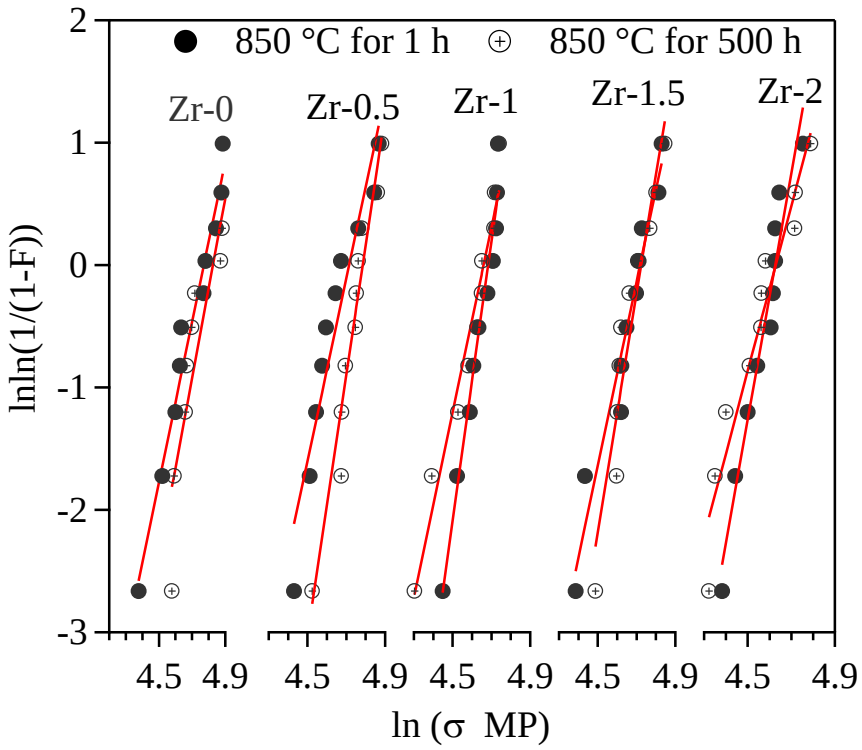

Figure S5: Weibull distribution of flexural strength for glass–powder compacts annealed at 850 ºC for 1h (filled symbols) and heat treated at 800 ºC for 500 h (open symbol).

In the present scenario, the shrinkage values varied between 13% and ~14%, confirming the good densification of glass powder compacts. The density values of GCs are well correlated with the density of the respective bulk glasses and increased with increasing ZrO_2 contents. It can be said that an insufficient amount of the residual glass phase, owing to the effective crystallization, might contribute for the remaining porosity left in the structure, because of the density difference between the glassy and crystalline phases.[8] The addition of ZrO_2 enhanced considerably both the glass shrinkage behavior and the densification degree. In order to characterize mechanical reliability of ZrO_2–containing melilite seals, the two–parameter Weibull strength distribution for the GCs sintered at 850 ºC for 1 h and 500 h are presented in Fig. S5. According to Weibull statistics, the increasing probability of failure (F) for a brittle material can be expressed by $F=1–exp\ (–\sigma/\sigma_0)^m$, where F is the failure probability for an applied stress (σ), σ_0 is a normalizing parameter known as Weibull characteristic strength, and m is the Weibull modulus. Here, the Weibull modulus m is a measure of the degree of strength data dispersion [9]. The bending strength values have been obtained from at least 10 different samples. It can be observed that the failure probability function provides a reasonable fit to the experimental data. A large Weibull modulus, called the shape factor m, relates to the uniformity of the distribution of flaws in a brittle material: a high value of m implies a highly uniform distribution of defect sizes and therefore a low level of variability of seal strengths. Conversely, a low value of m implies highly variable flaw sizes and a large spread of measured strengths. The relatively high Weibull modulus (m ~7–11) means good mechanical reliability for the sealants. The typical fracture surface of a bending strength tested specimen after heat treating for 500 h at 800 ºC were presented in Fig. S6. According to Griffith crack theory, when a propagating crack in the compound encounters a crystal with high strength and elastic modulus, the crack direction is

deviated by the crystal leading to an increase of the cleavage of the surface. As a result, a higher fracture surface energy is required for crack propagation. As observed from Fig. S6, the typical fracture surface of a bending strength tested specimen exhibits rough surfaces and thus may be having low crack growth energy.

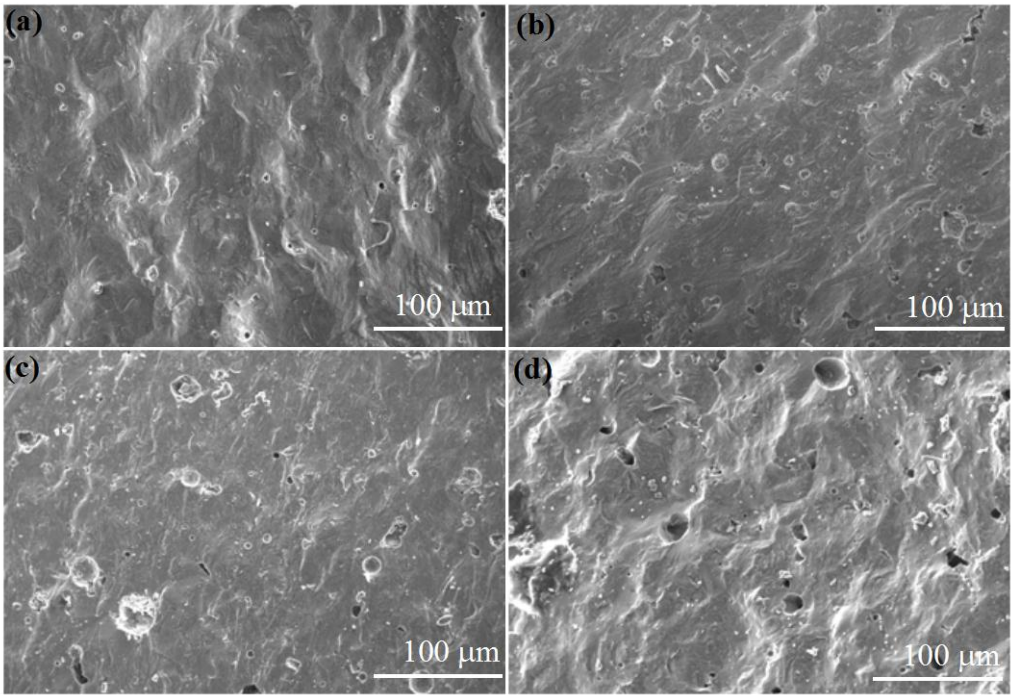

Figure S6: Fractured surfaces (a) Zr–1, (b) Zr–2, (c) Zr–3 and (d) Zr–4 GCs sintered at 850 ºC for 500 h after the 3 point bending strength measurement.

S6: Interaction studies

All the GC seals bonded well to Sanergy HT and Crofer22APU metallic interconnects with no gaps being observed, and the investigated interfaces showed homogeneous microstructures over their entire cross–sections of the joint. Fig. S7, shows the SEM image of the interfaces between Sanergy HT/Zr–4 GC along with the corresponding EDS elemental mappings of the relevant elements (Cr, Fe, Mn, Ca and Si) existing at the interface after heat treatment at

850 ºC for 1 h in air. Neither diffusion layers were detected at the interfaces by SEM/EDS analyses within the limits of experimental uncertainty.

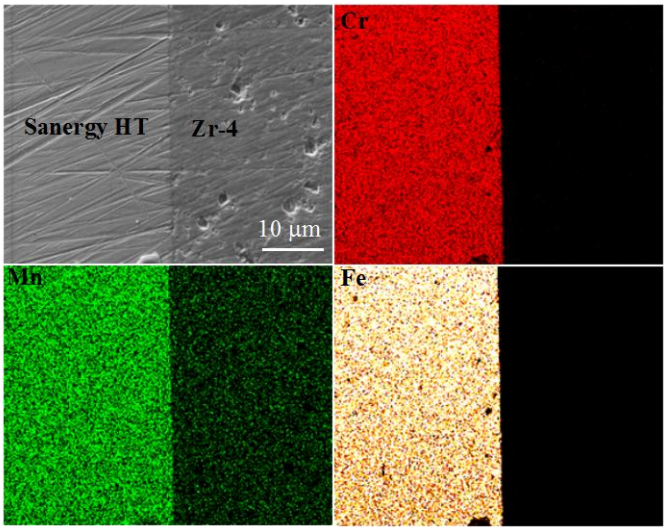

Figure S7: SEM image and EDS element mappings for Cr, Mn, and Fe, at the interface between Zr–4 and Sanergy HT after heat treatment at 850 ºC for 1 h

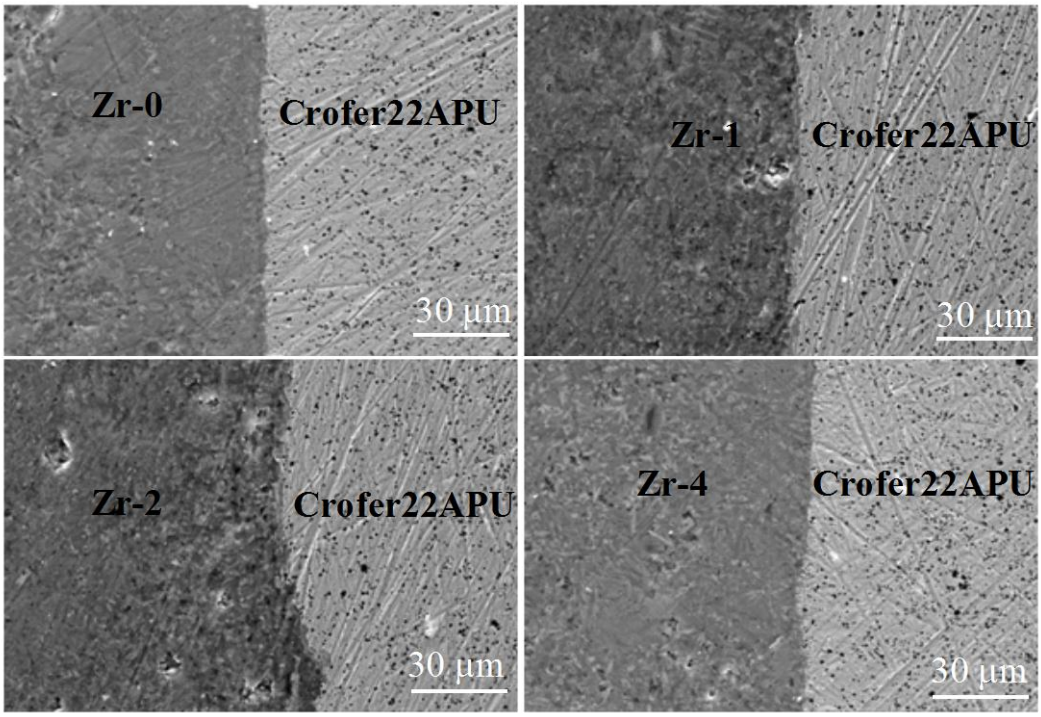

Figure S8: SEM images at the interface of (a) Zr–0 / Crofer22APU; (b) Zr–1 / Crofer22APU; (c) Zr–2 / Crofer22APU and (d) Zr–4 / Crofer22APU after heat treatment at 800 ºC for 500 h

References:

1. A. A. Reddy, D. U. Tulyaganov, S. Kapoor, A. Goel, M. J. Pascual, V. V. Kharton and J. M. F. Ferreira, *RSC Advances*, 2012, **2**, 10955.
2. A. A. Reddy, D. U. Tulyaganov, A. Goel, S. Kapoor, M. J. Pascual and J. M. F. Ferreira, *J. Mater. Sci.* 2013.
3. A. A. Reddy, D. U. Tulyaganov, M. J. Pascual, V. V. Kharton, E. V. Tsipis, V. A. Kolotygin and J. M. F. Ferreira, *Int.J. Hydrogen Energy*, 2013, **38**, 3073-3086.
4. D.W. Richerson, Marcel Dekker, Inc., New York, USA, 1992.
5. B. Luisa, C. Valeria, L. Cristina, M. Monia, M. Piercarlo and S. Cristina, *J. Phy. Chem. B*, 2003, **107**.
6. I. Lancellotti, C.Leonelli, M. Montorsi, G. C. Pellacani, C.Siligardi and C. Meneghini, *Phys. Chem. Glasses* 2002, **43C**, 1.
7. N. M. Bobkova, Zh. S. Tizhovka, V. V. Tizhovka, N. G. Cherenda, *J. Appl. Spectrosc.* 1979, **31**, 1556
8. M. Ghaffari, P. Alizadeh and M. R. Rahimipour, *J. Non-Cryst. Solids*, 2012, **358**, 3304-3311.
9. Allu Amarnath Reddy, Ashutosh Goel, Dilshat U. Tulyaganov, Saurabh Kapoor, K. Pradeesh, Maria J. Pascual and J. M. F. Ferreira, *J. Power Sources* 2013, **231**, 203-212.